

## Numerical Optimization and Noise Analysis of High-Tip-Speed Wind Turbine

Long Wang<sup>1,2</sup>, Guoping Chen<sup>2</sup>, Tongguang Wang<sup>1,\*</sup> and Jiufa Cao<sup>3</sup>

<sup>1</sup> Jiangsu Key Laboratory of Hi-Tech Research for Wind Turbine Design, Nanjing University of Aeronautics and Astronautics, Nanjing, Jiangsu 210016, China

<sup>2</sup> State Key Laboratory of Mechanics and Control for Mechanical Structures, Nanjing University of Aeronautics and Astronautics, Nanjing, Jiangsu 210016, China

<sup>3</sup> College of Energy and Power Engineering, Yangzhou University, Yangzhou, Jiangsu 225009, China

Received 6 November 2016; Accepted (in revised version) 23 January 2017

---

**Abstract.** With lower turbulence and less rigorous restrictions on noise levels, offshore wind farms provide favourable conditions for the development of high-tip-speed wind turbines. In this study, the multi-objective optimization is presented for a 5MW wind turbine design and the effects of high tip speed on power output, cost and noise are analysed. In order to improve the convergence and efficiency of optimization, a novel type of gradient-based multi-objective evolutionary algorithm is proposed based on uniform decomposition and differential evolution. Optimization examples of the wind turbines indicate that the new algorithm can obtain uniformly distributed optimal solutions and this algorithm outperforms the conventional evolutionary algorithms in convergence and optimization efficiency. For the 5MW wind turbines designed, increasing the tip speed can greatly reduce the cost of energy (COE). When the tip speed increases from 80m/s to 100m/s, under the same annual energy production, the COE decreases by 3.2% in a class I wind farm and by 5.1% in a class III one, respectively, while the sound pressure level increases by a maximum of 4.4dB with the class III wind farm case.

**AMS subject classifications:** 34H05, 45L05, 47F05, 76G25

**Key words:** Wind turbine design, high tip speed, multi-objective optimization, noise analysis.

---

## 1 Introduction

The tip speed of most commercially operating onshore wind turbines is usually limited to 80m/s, based on the consideration of both the power generation cost and the aerodynamic noise limitations of wind turbine. It is known that increasing the tip speed of wind

---

\*Corresponding author.

Email: tgwang@nuaa.edu.cn (T. G. Wang)

turbines will increase the aerodynamic noise [1, 2]. Although wind turbine noise limitations are not specified in IEC and GL standards, the tip speed is generally kept no higher than 80m/s to avoid causing considerable harm to the human population nearby wind farms. Nevertheless, increasing the tip speed brings a lot more benefits. For example, the wind speed range corresponding to the optimum rotor power coefficient can be expanded [3], thus promoting the power output of the wind turbine. In addition, increasing the tip speed will reduce the rotation moment acting on the blade as well as the loads acting on the drive train and generator, thus lowering the power generation cost [4].

The offshore wind turbine design may allow higher tip speed than onshore one. Because the sea is uninhabited by humans, there are less noise restrictions on noise propagation. Moreover, vertical air convection over an open sea is less violent and less affected by topographic factors; the turbulence intensity of offshore is much lower than that of onshore [5, 6]. Long-term field measurements of wind over an open sea can be found in the existing literature [7]. The characteristic value of the turbulence intensity at 15m/s I15 is 4.9% at the height of 90 m above sea level, which is much lower than the onshore turbulence intensity (minimum 12%) given in the IEC standard. This means that turbulent inflow noise, which is the main source of aerodynamic noise, greatly decreases for offshore wind turbines and therefore may leave much space for increasing the tip speed.

The optimization design of the wind turbine is in a process that involves many constraints, design variables and objectives among which there may exist conflicts with one another, whether the wind turbine tip speed is high or not. For large wind turbine design, a delicate balance must be achieved among several objectives including power generation cost and generating capacity [8]. A large number of design variables must be considered with respect to the aerodynamic configuration and the structural features as key components. Additionally, constraints are also needed to satisfy the requirements pertaining to geometry, loads, vibration and fatigue. Therefore, optimization design of large wind turbines is a multi-objective, multi-variable and multi-constraint problem. In the existing literature about wind turbine design [9], as many as 32 design variables and 102 constraint conditions are considered, making the optimization much challenging.

There exists no unique optimal solution for the multi-objective optimization of wind turbine design. Rather, the purpose of multi-objective optimization is to identify a group of trade-off solutions, known as Pareto optimal solutions, which are used to find the Pareto Front (PF). In essence, PF is the interface separating the feasible and infeasible solution regions in the objective space. Due to the complexity of the optimization, the multi-objective design of wind turbine currently uses evolutionary algorithms, including Hierarchical GA [10], PAES [11], SPEA2 [12, 13], MOGA [14], NSGA-II [15–18] and PSO [19, 20]. These algorithms are categorized as gradient-free algorithms (GFAs) [21]. The most salient advantage of GFAs is the tolerance of random errors generated in searching, which makes the algorithms suitable to optimization problems with any number of variables, objectives and constraints. However, when applied to complex multi-objective optimization, GFAs may have the defects of poor convergence, low efficiency and inability to find the precise PF [22–24]. The reasons are two-fold. First, the optimization

efficiency of GFAs deteriorates sharply as the number of design variables increases, as previous studies have shown [21, 25]. As the number of design variables increases, the number of evolutionary generations increases in a nearly quadratic manner. For wind turbine design, which usually requires over 10 design variables, thousands of evolutionary generations may be needed to obtain the desired result using GFAs. Given this defect, previous studies have attempted to improve the efficiency of single-objective optimization for wind turbines by means of various gradient-based mechanisms [26, 27], but gradient-based algorithms have not yet been successfully applied to the multi-objective optimization of wind turbines. The second major shortcoming of GFAs concerns their diversity preservation mechanisms, specifically clustering operators [10–13] and crowding distance [14–18], which have some intrinsic defects that may lead to unacceptable population distribution. Previous studies [22, 28] have shown that both diversity preservation mechanisms subject the population distribution to dynamic adjustment in each generation. This leads to performance fluctuation and low efficiency as well as population clustering due to failed diversity preservation mechanisms, so that a satisfactory PF may not be obtained.

Base on the above descriptions, convergence performance and optimization efficiency, the two crucial factors for optimization, are significantly challenging in cases where conventional GFAs are applied in multi-objective design of wind turbine. Making this issue worse, however, both of these factors tend to be ignored in wind turbine design. In this article, based on uniform decomposition and positive-gradient evolution, a high performance gradient-based differential evolution algorithm named as the MODE/D & P is proposed and described in detail. Using this algorithm, optimization is conducted for the design of several 5MW offshore wind turbines under different tip speeds. Furthermore, the effect of tip speed on power generation cost and annual energy production is discussed, followed by a noise analysis. To the best of our knowledge, this is the first time that gradient-based differential evolution algorithms have been used in the multi-objective design of wind turbines.

## 2 Overview of wind turbine multi-objective optimization process

The multi-objective optimization of large wind turbines under different tip speeds is comprised of four parts: input, simulation, optimization and validation, as shown Fig. 1.

In the input part, the shape, structure and material of each component of wind turbines, different tip speeds, design standard, as well as the basic parameters of the optimization algorithm are provided for commencing the optimization. In the part of simulation, the parametric modelling for the optimized components of wind turbines is carried out to generate the design variables. This modelling part will be described in detail in Section 3, where the aerodynamic performance of the wind turbine is also calculated using the blade element momentum theory. Determination of the extreme loads on

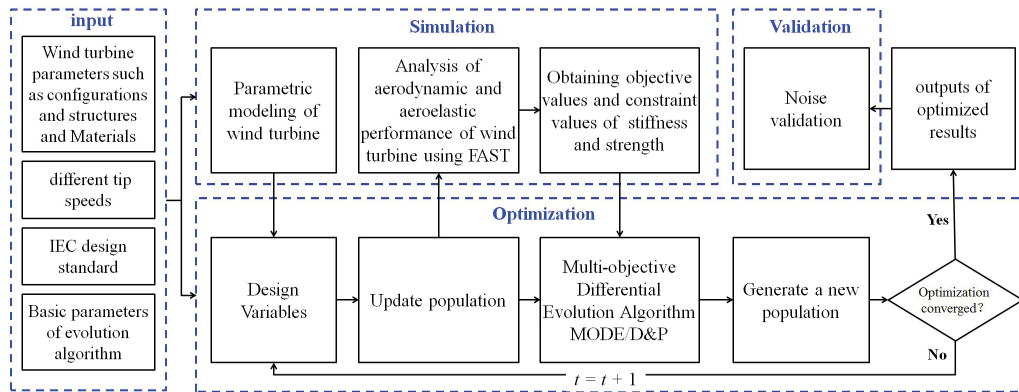


Figure 1: Workflow of a high-tip-speed wind turbine design.

the wind turbine, prerequisite for structural design, is a complicated and complex task involved in nonlinear simulations of aero-elastic-hydro-servo interactions in thousands of design load cases. In this study, the extreme loads are evaluated using the FAST codes [29] based on the IEC standard. The FAST codes are professional-grade and widely-used software packages for wind turbine performance analysis. The codes have been extensively tested and validated by many kinds of wind turbines [30, 31] and the calculation accuracy and reliability are widely recognized. In the part of optimization, a high-performance multi-objective optimization algorithm, named as MODE/D & P, is developed to deal with the complex optimization, based on decomposition and differential evolution. The algorithm will be described in detail in Section 4. In the validation part, comparative analyses of noise levels and propagation pattern to the two optimized wind turbines with the tip speeds of 80m/s and 100m/s, respectively, are launched based on a reliable semi-empirical noise prediction model.

The optimization procedures are as follows. First, the basic parameters of optimization are input; parametric modelling of the blades and tower of the wind turbine is performed and the design variables are determined. Then, the initial population for the optimization algorithm is generated randomly and a mechanical analysis of the entire wind turbine is performed in order to obtain the values of objectives and constraints. Then they are introduced into the MODE/D & P algorithm to generate a new population. Convergence is judged based on convergence criteria. If convergence is reached, the optimized result is obtained and the noise analysis is subsequently conducted for the optimized wind turbine; otherwise, the population is updated and the optimization continues for the  $(t+1)$ -th generation.

### 3 Modelling of wind turbine

### 3.1 Objective functions

#### 3.1.1 Minimum cost of energy

Cost of energy (COE), defined as the ratio of the total annual cost CTA to the annual energy production (AEP), is calculated using the model of the NREL CSM [32]. NREL CSM is the most extensively used cost analysis model for wind turbines [32]. It has been applied with high reliability to the cost analysis of several types of wind turbines, ranging from 750kW to 5MW [33, 34]. In the model, loads on each component are translated into costs by various pre-constructed empirical cost models. The calculation of the COE is given by

$$f_1 = \min COE = \min \frac{Fr \cdot (TCC + BOS) + (1 - \beta) \cdot OPEX}{AEP},$$

where TCC represents the turbine capital cost, BOS the balance-of-station costs and OPEX the operational expenditures;  $Fr$  is the financing rate and the tax deduction rate.

#### 3.1.2 Maximum annual energy production

Annual energy production (AEP) under a given wind farm condition is calculated using the following equation [8]:

$$f_2 = \max \sum_{i=1}^{N-1} \left( \frac{1}{2} (P(V_{i+1}) + P(V_i)) \times f(V_i < V < V_{i+1}) \times T \right),$$

$$f(V) = \frac{K}{C} \left( \frac{V}{C} \right)^{K-1} e^{-\left(\frac{V}{C}\right)^K},$$

where,  $P(V)$  is the output power at the wind speed  $V$ ,  $f(V)$  the Weibull distribution function,  $T$  the annual hours,  $K$  the scale parameter and  $C$  the shape parameter.

In order to validate the methods of power calculation and AEP calculation used in this study, the NREL Phase VI wind turbine [35] and the AERODYN-1.5MW wind turbine [18] are chosen as test samples. Fig. 2 provides a comparison of the calculated and experimental results of power output for the NREL Phase VI wind turbine. The power is calculated based on the blade element momentum (BEM) theory codes, which is developed by the authors and had been embedded into the optimization. As can be seen, the calculated results agree well with the experimental results over the entire wind speed range. This BEM method is then used to calculate the AEPs for the AERODYN-1.5 MW wind turbine at different annual mean wind speeds, which are compared with the results from the GH BLADED software, as shown in Fig. 3. The commercial software GH BLADED is widely used for wind turbine certification [25] in wind energy industry. The AEPs obtained from the aerodynamic model used in this optimization agrees well with the GH BLADED results with a maximum error of 0.8% at the annual mean wind speed of 10m/s.

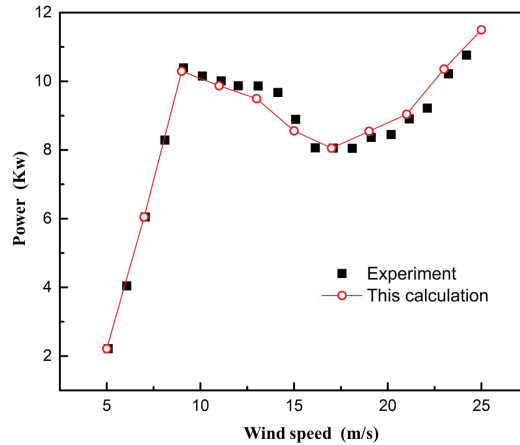


Figure 2: Comparison of calculated and measured output power on the NREL Phase VI wind turbine.

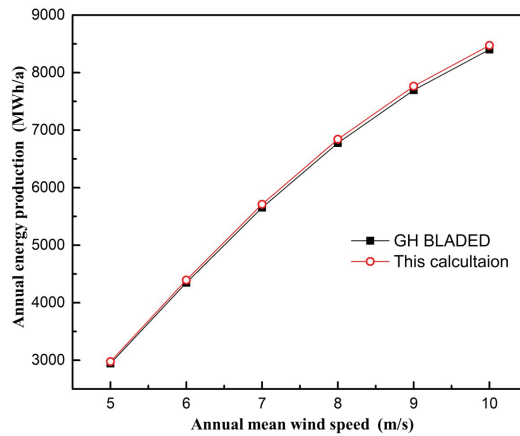


Figure 3: Comparisons of calculated AEP on the AeroDyn-1.5MW wind turbine.

### 3.2 Design variables

The optimizations in this study are conducted based on the NREL 5 MW baseline wind turbine [36]. Therefore, other than the blade and tower, the machine configuration, structures and materials of major components are all kept consistent with the NREL 5MW wind turbine. A total of 32 variables are constructed and expressed in the following

$$X = \{c, \theta, t_{relt}, d_{pre}, t_{spar}, t_{te}, d_{tower}\}.$$

The blade aerodynamic shape variables are used to describe the geometrical features of the blade including the distributions of chord ( $c$ ), twist ( $\theta$ ), relative thickness ( $t_{relt}$ ) and pre-bending ( $d_{pre}$ ). These variables determine the blade aerodynamic performance. In this study, the blade chord, twist and relative thickness distributions are, respectively,

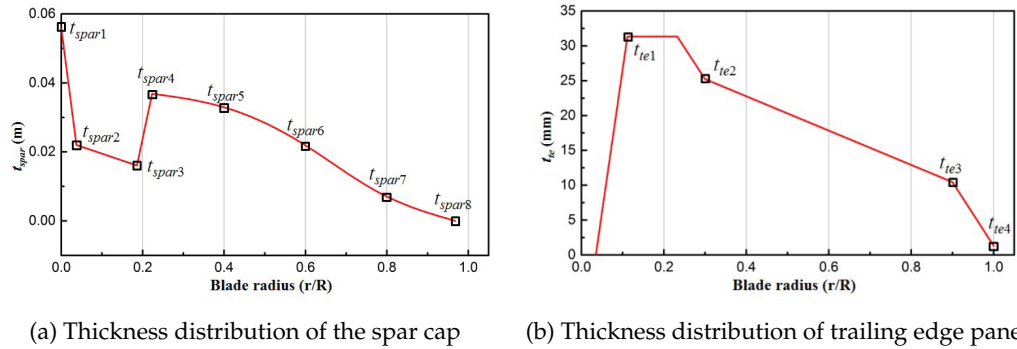


Figure 4: Definition of the structural variables of the blade.

defined with five control points as design variables at the locations of  $0.2R$ ,  $0.4R$ ,  $0.6R$ ,  $0.8R$  and  $0.96R$  in the spanwise direction ( $R$  represents the blade length). The relative thickness is fixed as 100% at the blade root. Third-order spline fitting is applied for the distributions of chord, twist and relative thickness. The pre-bending distribution is fitted by an exponential function with three variables at the locations of  $0.5R$ ,  $0.75R$  and  $R$  in the spanwise direction.

The complex structure of the blade is simplified based on engineering experience to allow optimization [29]. The thickness distributions of the spar cap ( $t_{spar}$ ) for the inboard part before the location of the maximum chord length and the part from the location of the maximum chord length to the blade tip are fitted using linear and three-order spline, respectively. Fig. 4(a) shows the thickness distribution of the spar cap with eight variables. Four variables are arranged at designated positions in the spanwise direction of the blade and connected to each other in a linear pattern, to determine the thickness distribution of the trailing edge panel ( $t_{te}$ ), as shown in Fig. 4(b).

The external radii of the tower top and bottom are kept unchanged and the thickness of the tower wall ( $d_{tower}$ ) is the variable to be optimized. Linear fitting is adopted with two variables.

### 3.3 Constraints

The distributions of the chord, twist and relative thickness decrease gradually from the location of maximum chord length to the blade tip. In addition, the strength and stiffness of the blade are also restricted.

#### 3.3.1 Strength constraint

According to the requirements of the IEC 61400-1 (2015) standard, the safety factor ( $SF$ ), defined as the ratio of the maximum stress allowed in the local area ( $[\sigma_i]$ ) to the stress at

the location  $i$  ( $\sigma_i$ ), must be greater than 1 on the entire blade [8], as follows:

$$SF = \min \frac{[\sigma_i]}{\sigma_i} \geq 1,$$

where

$$\begin{cases} [\sigma_i] = \frac{f_{k,i}}{\gamma_m \gamma_n}, \\ \sigma_i = \gamma_f F_{k,i}, \end{cases}$$

$F_k$  is the characteristic value for the load.  $f_k$  is the characteristic value of material properties.  $\gamma_k$  is the partial safety factor for loads,  $\gamma_m$  is the partial safety factor for materials and  $\gamma_n$  is the failure factor. These coefficients are all given according to the IEC standard.

### 3.3.2 Deflection constraint

The deflection of blades must be controlled to avoid striking the tower. According to the IEC standard, the minimum clearance ( $D_{c,\min}$ ) of the blade is greater than 30% of the initial clearance ( $D_c$ ), as in the following:

$$D_{c,\min} \geq 0.3 \cdot D_c.$$

## 4 Proposed optimization algorithm

In order to overcome the problems of poor convergence and low efficiency in the multi-objective optimization of a wind turbine, a new gradient-based multi-objective evolutionary algorithm, named as MODE/D & P, is proposed based on uniform decomposition and differential evolution. The procedure of the proposed algorithm is shown in Fig. 5. Uniformly distributed reference vectors are established in the objective space so that populations can approach the PF by surrounding these vectors and eventually converge at the intersections of these points and PF. A gradient-based differential evolution method is developed to significantly improve optimization efficiency.

### 4.1 Uniform decomposition mechanism for diversity preservation

At the initiation of MODE/D & P, a series of uniformly distributed reference vectors are set up in the objective space. These vectors are established in a hyper-cube with a unit size of 1 and thus are called normalized reference vectors (NRVs), as shown in Fig. 6. Anchor points are fixed at locations on axes with an intercept of 1 and a Utopia plane is established by connecting these points. Then, uniformly distributed Utopia points are identified on the Utopia surface and a series of lines that are perpendicular to the Utopia

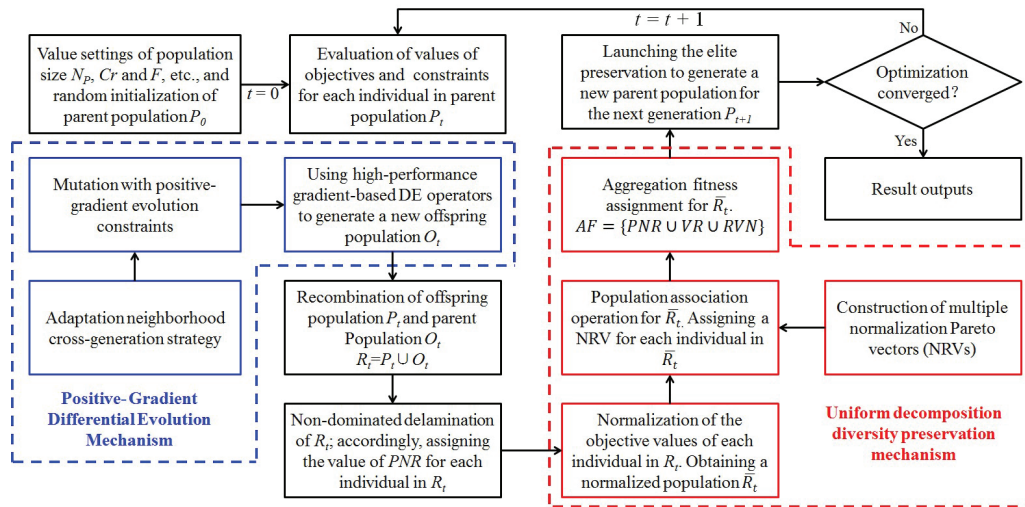


Figure 5: The MODE/D & P procedure.

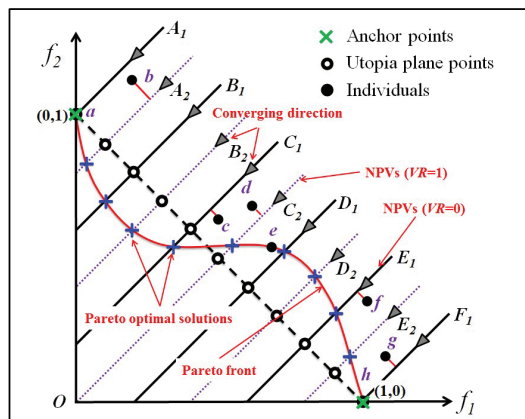


Figure 6: Schematic of multiple NRVs in two-objective optimization.

surface are identified to pass through the Utopia points. The quantity of NRVs ( $N_V$ ) can be obtained using the following equation:

$$N_V = C_{m+N_S-1}^{N_S}$$

where  $N_S$  is the number of divisions of each objective axis.

During the process of optimization, some vectors may not be linked to the individuals of the algorithm, while others may be linked to several, which can lead to degraded algorithm performance and even failure. In MODE/D & P, the concept of multiple NRVs is introduced to overcome this drawback. For two consecutive ranks of NRVs in two-objective optimization (see Fig. 6), NPVs in the second rank ( $A_2, B_2, C_2$ , etc.) are obtained

by doubling the NS in the first rank ( $\mathbf{A}_1, \mathbf{B}_1, \mathbf{C}_1$  etc.). The vector rank ( $VR$ ) of each rank is defined as 0 for the first rank and increased by 1 for each successive rank. More than two ranks are generated if necessary, but each rank is generated only once.

After the construction of the multiple NRVs needed, the association of populations with NRVs is achieved through three steps. First, the Euclidean distances between each individual and NRVs in the 0th rank are obtained and the label of the NRV corresponding to the minimum Euclidean distance is considered as a variable of the individual. Then, all the individuals associated with one specific reference vector ( $j$ ) are categorized in a subset. Finally, the individual with the shortest Euclidean distance in each subset is selected and the current  $VR$  value is attributed to that individual. The other individuals are then associated to the NRVs in the next rank until every individual is associated with a unique vector.

## 4.2 Positive-gradient differential evolution

### 4.2.1 Converging direction

Ideally, the Pareto optimal solutions should converge at the points where the reference vectors intersect with the PF (see Fig. 6). Therefore, the most effective converging pattern involves individuals approaching the PF along reference vectors. For minimization, the converging directions of each individual are defined as the direction toward the origin along the respective reference vectors.

### 4.2.2 Positive-gradient constraints

The positive-gradient constraint is a novel scheme proposed in this study in order to enhance the searching ability of the algorithm. The advance vector  $\mathbf{V}_{i,adv,g}$  in the objective space is mapped from the trial vector  $\mathbf{V}_{i,trial,g}$  in the variable space. If the direction of the advance vector deflects from the converging direction of the reference vector  $\mathbf{U}_i$ , the most likely reason is the performance degradation of the reference individual and the failure of this evolution. Therefore, constraining the angle between the trial vector and the positive converging direction to below 90 degrees is the best way to guarantee the positive evolution of the individual. Subsequently, the positive-gradient mutation is established based on a classical "DE/best/1" scheme and a neighbourhood cross-generation scheme [37]:

$$\begin{aligned}\mathbf{X}_{i,g} &= \mathbf{X}_{i,best,g} + F \cdot \mathbf{V}_{i,trial,g}, \\ \mathbf{V}_{i,adv,g} &= \mathbf{Y}_{i,rn1,g} - \mathbf{Y}_{i,rn2,g-1},\end{aligned}$$

which satisfies:

$$\begin{cases} \mathbf{V}_{i,trial,g} = \mathbf{X}_{i,rn1,g} - \mathbf{X}_{i,rn2,g-1}, & \text{if } \mathbf{V}_{i,adv,g} \cdot \mathbf{U}_i \geq 0, \\ \mathbf{V}_{i,trial,g} = \mathbf{X}_{i,rn2,g} - \mathbf{X}_{i,rn1,g-1}, & \text{if } \mathbf{V}_{i,adv,g} \cdot \mathbf{U}_i < 0, \end{cases}$$

where  $\mathbf{X}_{i,rn1,g}$  is an individual that is randomly selected from the NSP of the current generation associated with the vector  $i$ ,  $\mathbf{X}_{i,rn2,g-1}$  is an individual that is randomly selected

from the NSP of the previous generation and  $Y_{i,rn1,g}$  and  $Y_{i,rn2,g-1}$  corresponding to  $X_{i,rn1,g}$  and  $X_{i,rn2,g-1}$  are the vectors of the objective values.  $F$  is the scale factor.

### 4.3 Parameter adaptation scheme

In classical differential evolution algorithms, the scale factor and crossover rate ( $Cr$ ), both of which are constant, are the two key factors reflecting the evolution step of individuals in every generation. The self-adaptability of these two factors can boost optimization efficiency and universal capability of the algorithm because of its significant effects on the differential evolution algorithms. A highly effective parameter adaptation scheme, which has been reported elsewhere [37] is employed in this study. The equation is as follows:

$$F_{i,g} = mean_A(NF_{i,n,g} \cup NF_{i,n,g-1}) + \theta_F \cdot Gaussian(0,1),$$

$$Cr_{i,g} = mean_A(NCr_{i,n,g} \cup NCr_{i,n,g-1}) + \theta_{Cr} \cdot Gaussian(0,1),$$

where  $F_{i,g}$  and  $Cr_{i,g}$  are, respectively, the scale factor and crossover rate that correspond to the  $i$ th vector in differential evolution,  $MeanA(NF_{i,n,g} \cup NF_{i,n,g-1})$  and  $MeanA(NCr_{i,n,g} \cup NCr_{i,n,g-1})$  are the mean value of the scale factor and the crossover rate of all of the individuals in NSPs of the two consecutive generations, respectively,  $Gaussian(0,1)$  is the Gaussian distribution function and  $\theta_F$  and  $\theta_{Cr}$  are the constant coefficients of the scale factor and crossover rate, respectively.

## 5 Results and analysis

The 5MW wind turbine designs are conducted for Class I and Class III wind sites with the annual mean wind speed of 10m/s and 7.5m/s, respectively. The tip speeds are 80, 90 and 100m/s, respectively. The optimization objectives are the minimum COE and maximum AEP. The population size and evolution generation for the optimization are set to be 20 and 300, respectively. The wind turbine basic parameters are set the same as the NREL 5MW baseline wind turbine except for the design variables to be optimized, as mentioned in Section 3.2.

### 5.1 performance of optimization algorithm

To demonstrate the performance of the optimization algorithm, the results of the 5MW wind turbine designs are analysed here only for Class I wind site and the tip speed of 80m/s. A comparison of the MODE/D & P is made with the NSGA-II [15], which is the most widely used algorithm in multi-objective optimization of wind turbines. The hypervolume indicator ( $I_{HV}$ ) [38] is used to quantitatively evaluate the convergence and diversity of optimization algorithms. A higher  $I_{HV}$  value indicates a good approximation of the optimal solutions to PF and an excellent distribution of the optimal solutions.

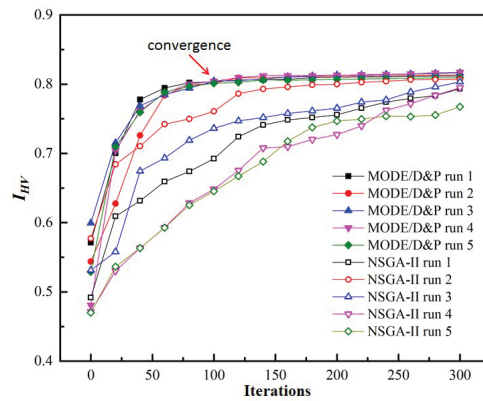


Figure 7:  $I_{HV}$  values obtained by 5 runs using the two algorithms.

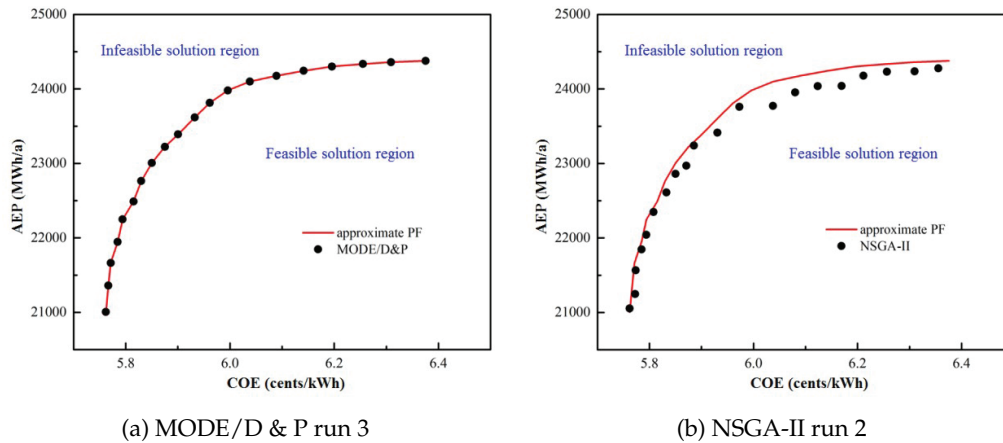


Figure 8: Comparison of the distribution of optimal solutions with the two algorithms.

Fig. 7 shows the  $I_{HV}$  values of 300 generations obtained for different 5 runs using MODE/D & P and NSGA-II algorithms, respectively. Although the starting point of evolution differs, the  $I_{HV}$  values basically coincide at the 120th generation in the all 5 runs using the MODE/D & P algorithm. Thereafter, they remain stable, indicating that the algorithm can reach convergence quickly and stably. In contrast, with the NSGA-II algorithm, the  $I_{HV}$  values differ significantly in the 5 runs, demonstrating that the convergence of the NSGA-II algorithm is very unstable. The  $I_{HV}$  value is obviously lower using the NSGA-II algorithm than that using MODE/D & P algorithm after 300 generations, indicating that the NSGA-II algorithm is difficult to reach a convergence.

The best results achieved for the 5MW wind turbine optimization using the MODE/D & P algorithm and the NSGA-II algorithm, respectively, are given in Fig. 8, where the distributions of the optimal solutions are compared in the objective space. Each point on the curve represents an optimal design. The optimal solutions compose a monoton-

ically increasing curve (represented by the solid line, called approximate PF), which indicates the conflict of the two objectives; as COE is reduced, AEP will inevitably decline. The MODE/D & P algorithm obtains a set of approximately uniformly distributed optimal solutions. However, the optimal solutions obtained by the NSGA-II algorithm are slightly clustered, without converging to the approximate PF. Correspondingly, the lower value of  $I_{HV}$  with the NSGA-II algorithm results from its poor convergence and diversity preservation performance. Therefore, compared to the NSGA-II algorithm, the MODE/D & P can significantly improve the convergence performance and diversity of optimal solutions.

### 5.2 Design results at different tip speeds

Two-objective optimizations for the 5MW wind turbine under three tip speeds of 80, 90 and 100m/s are given and the effect of tip speed on power generation cost and power output is discussed here.

The distributions of optimal solutions for the 5MW wind turbine under the three tip speeds are compared in Fig. 9, where the AEP and COE of the NREL-5MW wind turbine are also marked. The most significant trend is that, as the tip speed increases, PF shifts towards lower COE in the objective space.

To explain the reasons for this shift, the AEP of the NREL-5MW wind turbine is taken as a reference and three optimization designs (A, B and C corresponding to the tip speeds of 80, 90 and 100m/s, respectively) with very similar AEP are chosen from the three PFs for further analysis. The operational parameters and performance of the three designs are given in Fig. 10. As can be seen, the COEs of all the three designs are significantly lower than the COE of the real NREL-5MW wind turbine. The NREL 5MW wind turbine is not considered as an optimal design [36] since its high chord distribution leads to considerable extreme load and therefore increases the COE.

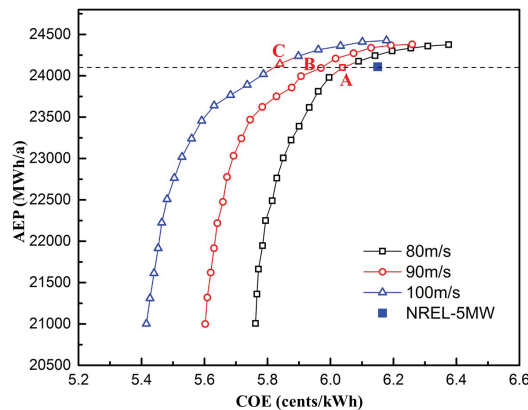


Figure 9: Optimal solutions for the 5MW wind turbines in Class I wind farm.

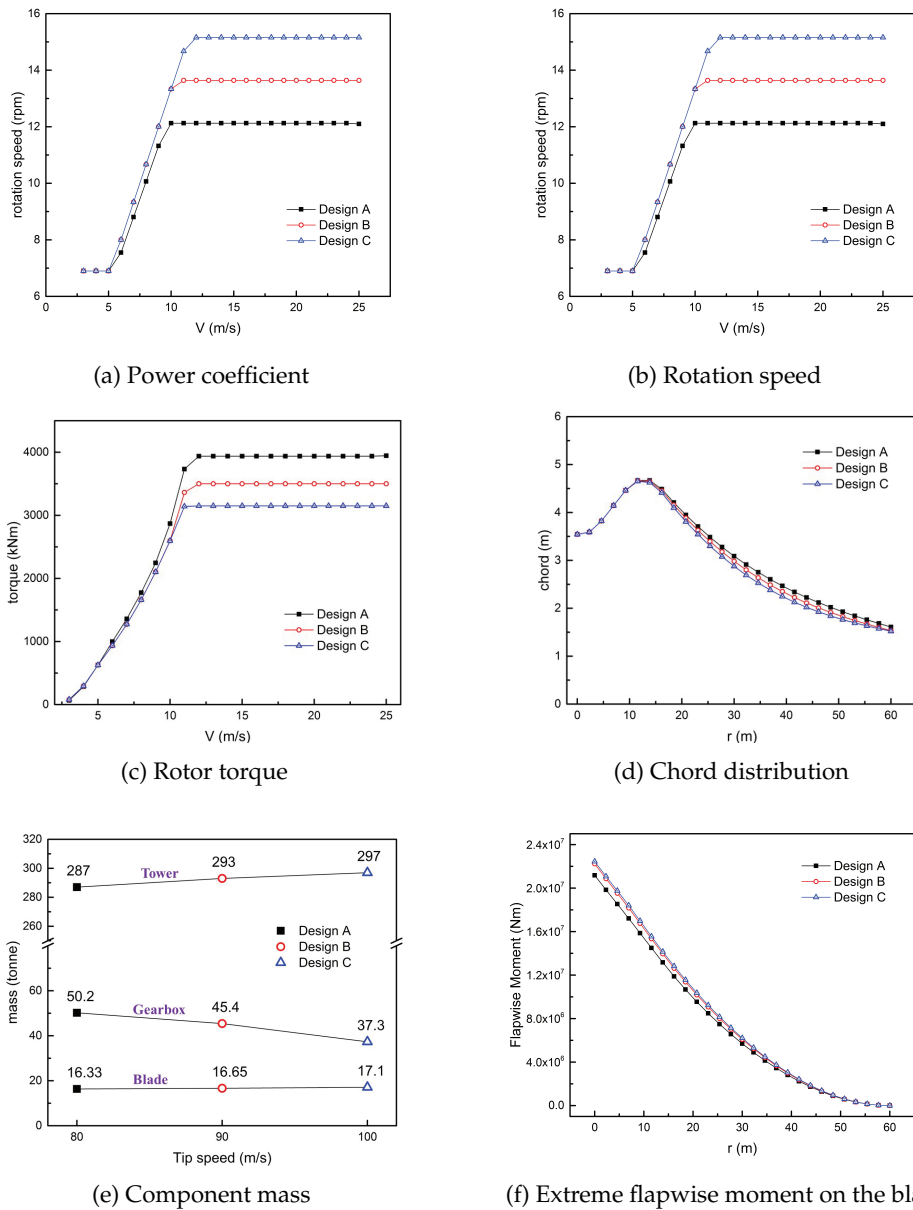


Figure 10: Operational parameters and performance of the designs A, B and C.

The power coefficients are almost identical for Design A and C (Fig. 10(a)). As the tip speed increases from 80m/s in Design A to 100m/s in Design C, the rated rotational speed of the rotor increases from 12.1rpm to 15.1rpm (Fig. 10(b)), while the rotor torque remarkably decreases from xx to xx kNm (Fig. 10(c)). Nevertheless, the rated power of 5MW is achieved for the designs. This brings about two major benefits. First, the blade

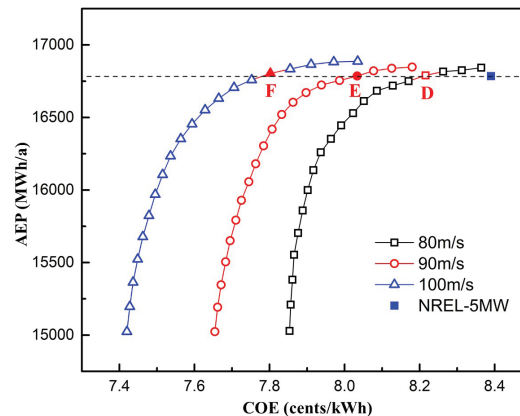


Figure 11: Optimal solutions for the 5 MW wind turbines in Class III wind farm.

chord can be shortened at a lower rotor torque (Fig. 10(d)), which is very important for reducing the loads on the turbine. Second, the gearbox speed ratio and gearbox weight can be greatly reduced at higher blade rotational speed. The gearbox weight in Design C is lower than that in Design A by 25.7% (Fig. 10(e)), resulting in a considerable reduction of the total turbine cost. However, the extreme loads of the turbine will increase at higher tip speed. The blade root flapwise moment in Design C is increased by 6% compared to that in Design A (Fig. 10(f)), which results in a 4.7% increase in blade weight (Fig. 10(e)) and a 3.4% increase in the weight of the tower. The compromise of the advantages and the adverse impact of increasing the tip speed ultimately results in a decrease of COE in Design C by 3.2% compared to that in Design A.

Design A can be compared with design B in the same way and the COE of Design B decreases by 1.2% compared to that of Design A.

The similar optimization is conducted for a Class III wind farm, where the annual mean wind speed is 7.5m/s. The distribution of optimal solutions obtained at different tip speeds is given in Fig. 11 and the operational parameters and performance of the designs D, E and F, chosen from the optimal solutions corresponding to the tip speeds of 80, 90 and 100m/s, respectively, are compared in Fig. 12.

Increasing the tip speed can also reduce the COE in the Class III wind farm; the trend observed is very similar to that in the Class I wind farm given above, except for two major differences. First, the COE of the turbine in Class III wind farm is considerably higher than that in Class I wind farm. This is because the masses of the blade, tower and gearbox, which are closely related to the COE (Fig. 12(d)), as well as the extreme load acting on the turbine (Fig. 12(f)) only decrease slightly as compared with those in Class I wind farm. In contrast, the AEP decreases dramatically in Class III wind farm due to the low annual mean wind speed. On the other hand, increasing the tip speed in Class III wind farm causes a more significant decrease in the COE. The COE of Design F is lower than that of Design D by 5.1% for this Class III wind farm, while this decrease is 3.2% in

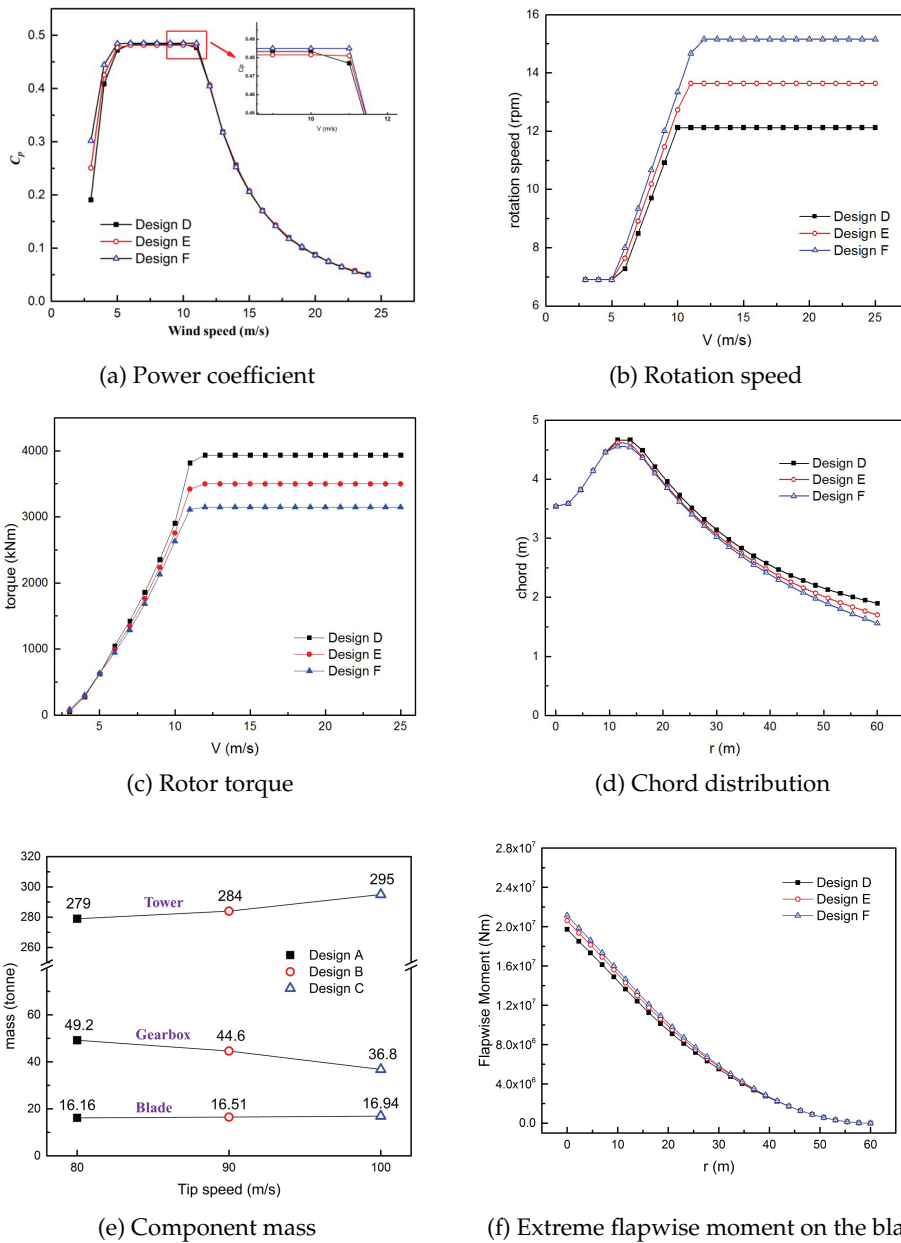


Figure 12: Operational parameters and performance of the turbine in designs D, E and F.

Class I wind farm as mentioned above, when the tip speed is increased to 100m/s from 80m/s. Therefore, increasing tip speed is more favourable for reducing the COE in a low-speed wind farm.

## 6 Noise analysis

### 6.1 Noise prediction model

A semi-empirical aerodynamic noise prediction model [39] is used to analyze the effect of tip speed on wind turbine noise. The model consists of three independent submodules to analyze noise sources with different characteristics. Total aeroacoustic noise from the wind turbine is then obtained by superposition.

Turbulent boundary layer trailing edge (TBL-TE) noise is generated by the spatial and temporal fluctuations of the pressure field due to the interaction between the turbulent boundary layer and the trailing edge. TBL-TE noise is predicted by the following equation:

$$SPL_{TBL-TE} = 10\log(10^{SPL_p/10} + 10^{SPL_s/10} + 10^{SPL_\alpha/10}),$$

where  $SPL_p$  is the noise generated from the pressure side of the blade,  $SPL_s$  is the noise generated from the suction side and  $SPL_\alpha$  is the noise caused by boundary layer separation. These three terms are given by:

$$\begin{aligned} SPL_p &= 10\log\left(\frac{\delta_p M^5 L D_h}{r_e^2}\right) + A\left(\frac{St_p}{St_1}\right) + (K_1 - 3) + \Delta K_1, \\ SPL_s &= 10\log\left(\frac{\delta_s M^5 L D_h}{r_e^2}\right) + A\left(\frac{St_s}{St_1}\right) + (K_1 - 3), \\ SPL_\alpha &= 10\log\left(\frac{\delta_s M^5 L D_h}{r_e^2}\right) + B\left(\frac{St_s}{St_2}\right) + K_2, \end{aligned}$$

where,  $\delta_p$  and  $\delta_s$  are the boundary layer displacement thickness of pressure and suction side,  $M$  is the Mach number,  $L$  is the span of the blade element,  $r_e$  is the effective observer distance,  $A$  is an empirical spectral shape,  $St_p$ ,  $St_s$ ,  $St_1$  and  $St_2$  are the Strouhal numbers representing different empirical relations,  $K_1$ ,  $K_2$  are the amplitude functions and  $\Delta K$  is the level adjustment amplitude function.  $D_h$  is the directivity function for high-frequency noise sources, as follows:

$$D_h(\Theta_e, \Phi_e) = \frac{2\sin^2\left(\frac{\Theta_e}{2}\right)\sin^2\Phi_e}{(1 + M\cos\Theta_e)(1 + (M - M_c)\cos\Theta_e)^2},$$

where  $M_c$  is the convective Mach number.  $\Theta_e$  and  $\Phi_e$  are the directivity angles, respectively.

Turbulent inflow (TI) noise is generated by the interaction between atmospheric turbulence and the leading edge of the turbine blade. Low-frequency and high-frequency

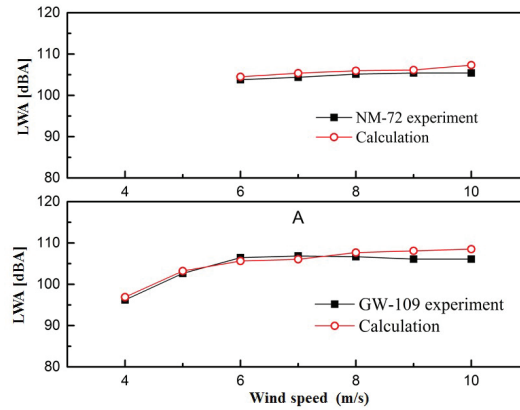


Figure 13: Comparison of the LWA of two wind turbines.

TI noises are predicted with the following equations, respectively [40]

$$SPL_{TI}^H = 10 \log \left( \frac{\rho_0^2 c_0^2 l L}{2r_e^2} M^3 U^2 I^2 \frac{K^3}{(1+K^2)^{7/3}} D_L \right) + 58.4,$$

$$SPL_{TI}^L = SPL_{in}^H + 10 \log \left( \frac{LFC}{1+LFC} \right),$$

where,  $\rho_0$  is the air density,  $c_0$  is the sound speed,  $l$  is the turbulence length scale,  $I$  is the turbulence intensity,  $K$  is the local wave number,  $D_L$  is a low-frequency directivity function and  $LFC$  is a low-frequency correction factor, as follows:

$$LFC = 10S^2 MK^2 (1 - M^2)^{-1},$$

$S$  is the compressible Sears function, its equation is as follows:

$$S^2 = \left( \frac{2\pi K}{1 - M^2} + \left( 1 + 2.4 \frac{K}{1 - M^2} \right)^{-1} \right)^{-1}.$$

Blade tip (BT) noise is a radiated noise caused by the interaction between the 3D tip vortex and the blade tip, calculated by the following equation [41]:

$$SPL_{Tip} = 10 \log \left( \frac{M^2 M_{max}^5 \gamma^2 D_h}{1 + LFC} \right) - 30.5 (\log St_d + 0.3)^2 + 126,$$

where,  $M_{max}$  is the maximum Mach number,  $\gamma$  is the spanwise extent of the separation zone and  $St_d$  is the Strouhal number based on  $\gamma$ . More detailed introductions about the models and parameters are in [39] to [41].

In order to validate the prediction accuracy of the noise model, a series of noise trial calculations for the two wind turbines with different power levels (NT-72 1.5MW [42]

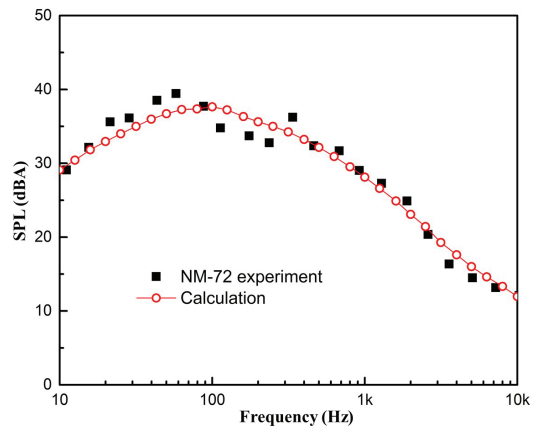


Figure 14: Comparison of one-third octave band spectrum at 6m/s.

and GW-109 2.5MW [43]) are carried out. Fig. 13 shows the comparison of the calculated and measured results for the sound power level (LWA) of the two wind turbines. The calculated total noise level agrees well with the experimental results with maximum errors being 1.9dB and 2.4dB, respectively. Fig. 14 shows the comparison of the calculated and measured sound pressure level (SPL) spectra at the wind speed of 6m/s. It is observed that minor discrepancies exist in some frequency ranges between the calculated and measured results, possibly resulting from the mechanical noise not included in the aerodynamic noise prediction model, as stated in [42]. Nevertheless, this has little impact on the overall *SPL* of the wind turbine, resulting in a difference of only about 1.2dBA.

## 6.2 Noise analysis for the optimized wind turbines

Increasing the tip speed of the wind turbine definitely increase noise emission from the turbine. To quantitatively evaluate the effect of increasing tip speed on wind turbine noise, Design A and C in the Class I wind farm with tip speeds of 80m/s and 100m/s, respectively, are chosen for comparison.

The changes in overall sound pressure level (OASPL) with wind speed in Design A and C are compared in Fig. 15. The reference turbulence intensity  $I_{15}$  is 5%, specifically set as same as the field measurement of an offshore wind farm [44]. The observation point on the ground for noise prediction is located at the position of  $(D/2+H)$  downstream from the tower ( $D$  is the rotor diameter and  $H$  is the tower height), according to the IEC standard. Generally, the OASPL of the two turbines first increases rapidly with the increase of wind speed. The increase of OASPL then slows down above the rated wind speed of 11m/s because the angle of attack of the blade is essentially constant by the pitch movement. The OASPL of Design C increases by a maximum of 4.4dB as compared with Design A at the wind speed of 14m/s.

Fig. 16 shows the 1/3 frequency octave spectra of SPL for different noise sources at

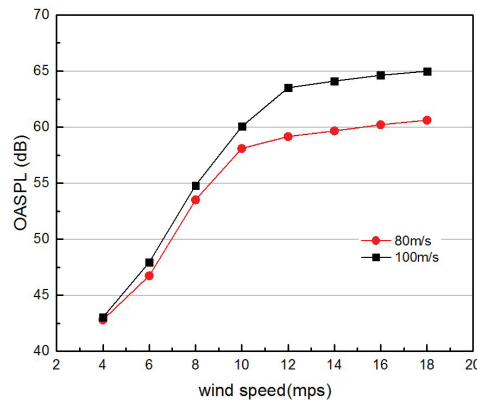
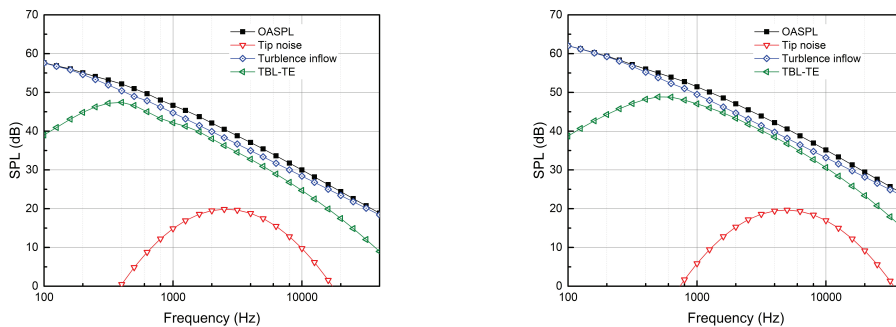


Figure 15: Comparison of the OASPL of design A and design C.



(a) Design A with a tip speed of 80m/s

(b) Design C with a tip speed of 100m/s

Figure 16: 1/3 octave band spectra of SPL for different noise sources at the wind speed of 12m/s.

the wind speed of 12m/s. As can be seen, within the frequency range, the turbulent inflow noise is dominant among all the noise sources. The TBL-TE noise also contributes significantly to the OASPL beyond 500Hz. The BT noise is small and its maximum SPL does not exceed 20dB. Comparison of design A and design C shows that increasing the tip speed increases the TI noise and TBL-TE noise beyond 500Hz. Though the BT noise generally shifts towards the middle-high frequencies, the maximum SPL of the BT noise is little influenced by increasing the tip speed.

Fig. 17 shows the footprints of OASPL at the wind speed of 12m/s for designs A and C. Turbulent inflow noise is not included in the figures, since it do not alter with respect of blade shape changes. It is clearly seen that the turbine noises show an approximately symmetrical radiation pattern in both the upwind and downwind directions on the rotor plane for the either design. The lowest noise occurs on the left and right sides of the rotor plane. While the SPL at each position in design C is higher than that in design A, the radiation patterns of noise do not differ significantly between the two designs.

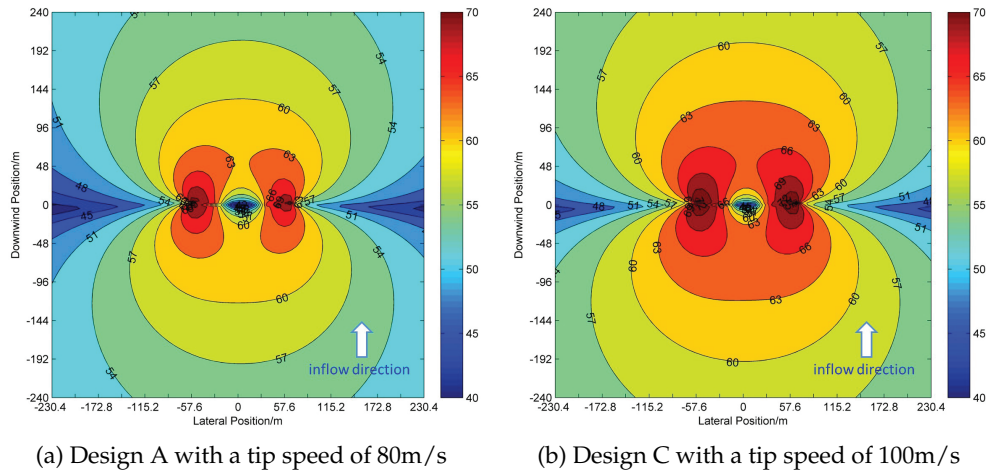


Figure 17: SPL footprints at the wind speed of 12m/s (blade self-noise).

## 7 Conclusions

Multi-objective optimizations of wind turbine have been carried out for high tip speed to lower the cost of energy. For the optimization, the gradient-based evolutionary algorithm has been proposed with uniform decomposition and differential evolution, so that uniformly distributed optimal solutions can be obtained with better convergence and optimization performance than the NSGA-II algorithm. The proposed algorithm has then been applied to the optimization design of the 5MW turbine at three tip speeds of 80, 90 and 100m/s. The results show that increasing the tip speed can reduce the wind power generation cost. As the tip speed increases from 80m/s to 100m/s, the COE decreases by 3.2% in a Class I wind farm and 5.1% in a Class III wind farm, respectively, under the same AEP. Finally, the noise analysis on the designs indicates that turbulence inflow noise predominates among all aeroacoustic noise sources of the wind turbine. As the tip speed increases from 80m/s to 100m/s, the noise increases by 4.4dB maximally. Therefore, the high-tip-speed wind turbine design is beneficial to the exploitation of offshore wind farms, which are of much low turbulence intensity and usually uninhabited by human beings.

## Acknowledgements

This work was funded by the National Basic Research Program of China (973 Program) (No. 2014CB046200), the National Nature science Foundation (No. 51506089), the Jiangsu Provincial Natural Science Foundation (No. BK20140059) and the Priority Academic Program Development of Jiangsu Higher Education Institutions.

## References

- [1] Y. GUO, T. PARSONS, K. DYKES AND R. N. KING, *A systems engineering analysis of three-point and four-point wind turbine drivetrain configurations*, Wind Energy, Published online in Wiley Online Library (wileyonlinelibrary.com), 2016.
- [2] B. R. RESOR, D. C. MANIACI, J. C. BERG AND P. RICHARDS, *Effects of increasing tip velocity on wind turbine rotor design*, Sandia National Laboratories: SAND2014-3136 518390, 2013.
- [3] S. GANJEFAR, A. A. GHASSEMI AND M. M. AHMADI, *Improving efficiency of two-type maximum power point tracking methods of tip-speed ratio and optimum torque in wind turbine system using a quantum neural network*, Energy, 67 (2014), pp. 444–453.
- [4] A. R. NEJAD, Y. GUO, Z. GAO AND T. MOAN, *Development of a 5MW reference gearbox for offshore wind turbines*, Wind Energy, 19 (2015), pp. 1089–1106.
- [5] L. ARANY, S. BHATTACHARYA, J. MACDONALD AND S. J. HOGAN, *Simplified critical mudline bending moment spectra of offshore wind turbine support structures*, Wind Energy, 18 (2015), pp. 2171–2197.
- [6] H. WANG, R. J. BARTHELMIE, S. C. PRYOR AND H. G. KIM, *A new turbulence model for offshore wind turbine standards*, Wind Energy, 17 (2014), pp. 1587–1604.
- [7] M. TÜRK AND S. EMEIS, *The dependence of offshore turbulence intensity on wind speed*, J. Wind Eng. Indust. Aerodyn., 98 (2010), pp. 466–471.
- [8] A. CHEHOURI, R. YOUNES, A. ILINCA AND J. PERRON, *Review of performance optimization techniques applied to wind turbines*, Appl. Energy, 142 (2015), pp. 361–388.
- [9] J. S. GRAY, T. A. HEARN, K. T. MOORE, J. T. HWANG, J. R. MARTINS AND A. NING, *Automatic evaluation of multidisciplinary derivatives using a graph-based problem formulation in Open MDAO*, 15th AIAA/ISSMO Multidisciplinary Analysis and Optimization Conference, Atlanta, Georgia, USA, 2014.
- [10] P. P. GIGUÈRE, M. S. SELIG AND J. L. TANGLER, *Blade design trade-offs using low-lift airfoils for stall-regulated HAWTs*, J. Solar Energy Eng., 121 (1999), pp. 217–223.
- [11] E. BENINI AND A. TOFFOLO, *Optimal design of horizontal-axis wind turbines using blade-element theory and evolutionary computation*, J. Solar Energy Eng., 124 (2002), pp. 357–363.
- [12] A. KUSIAK, Z. ZHANG AND M. LI, *Optimization of wind turbine performance with data-driven models*, IEEE Transactions on Sustainable Energy, 1 (2010), pp. 66–76.
- [13] R. DUFO-LOPEZ, *Multi-objective optimization minimizing cost and life cycle emissions of stand-alone PV-wind-diesel systems with batteries storage*, Appl. Energy, 88 (2011), pp. 4033–4041.
- [14] Y. P. JU AND C. H. ZHANG, *Multi-point robust design optimization of wind turbine airfoil under geometric uncertainty*, Proceedings of the Institution of Mechanical Engineers Part A Journal of Power & Energy, 226 (2012), pp. 245–261.
- [15] L. WANG, T. G. WANG AND Y. LUO, *Improved non-dominated sorting genetic algorithm (NSGA)-II in multi-objective optimization studies of wind turbine blades*, Appl. Math. Mech., 32 (2011), pp. 739–748.
- [16] M. SESSAREGO, *A hybrid multi-objective evolutionary algorithm for wind-turbine blade optimization*, Eng. Opt., 47 (2015), pp. 1043–1062.
- [17] S. Y. D. SORKHABI, D. A. ROMERO, G. K. YAN, M. D. GU, J. MORAN, M. MORGENROTH AND C. H. AMON, *The impact of land use constraints in multi-objective energy-noise wind farm layout optimization*, Renewable Energy, 85 (2016), pp. 359–370.
- [18] W. WANG, S. CARO, F. BENNIS, R. SOTO AND B. CRAWFORD, *Multi-objective robust optimization using a postoptimality sensitivity analysis technique: application to a wind turbine design*, J. Mech. Design, 137 (2015), 011403-1-11.

- [19] C. C. LIAO, X. L. ZHAO AND J. Z. XU, *Blade layers optimization of wind turbines using FAST and improved PSO algorithm*, *Renew Energy*, 42 (2012), pp. 227233.
- [20] M. SHARAFI, T. Y. ELMekkawy AND E. L. BIBEAU, *Optimal design of hybrid renewable energy systems in buildings with low to high renewable energy ratio*, *Renewable Energy*, 83 (2015), pp. 1026–1042.
- [21] A. NING AND D. PETCH, *Integrated design of downwind land-based wind turbines using analytic gradients*, *Wind Energy*, Published online in Wiley Online Library (wileyonlinelibrary.com), 2016.
- [22] C. LUCKEN, B. BARAN AND C. ABRIZUELA, *A survey on multi-objective evolutionary algorithms for many-objective problems*, *Comput. Opt. Appl.*, 58 (2014), pp. 707–756.
- [23] R. BAÑOS, F. MANZANO-AGUGLIARO, F. G. MONTOYA, C. GIL, A. ALCAYDE AND J. GÓMEZ, *Optimization methods applied to renewable and sustainable energy: A review*, *Renewable & Sustainable Energy Reviews*, 15 (2011), pp. 1753–1766.
- [24] B. CHANG, A. MILLER, R. ISSA AND G. CHEN, *Review of computer-aided numerical simulation in wind energy*, *Renewable & Sustainable Energy Reviews*, 25 (2013), pp. 122–134.
- [25] X. WANG, W. Z. SHEN, W. J. ZHU, J. N. SRENSSEN AND C. JIN, *Shape optimization of wind turbine blades*, *Wind Energy*, 12 (2009), pp. 781–803.
- [26] D. H. WOOD, *Dual purpose design of small wind turbine blades*, *Wind Eng.*, 28 (2004), pp. 511–527.
- [27] S. ABEDI, *A comprehensive method for optimal power management and design of hybrid RES-based autonomous energy systems*, *Renewable & Sustainable Energy Reviews*, 16 (2012), pp. 1577–1587.
- [28] T. WAGNER, N. BEUME AND B. NAUJOKS, *Pareto-, aggregation- and indicator-based methods in many-objective optimization*, *Int. Conference Evolutionary Multi-Criterion Optimization*, 2007.
- [29] B. R. RESOR AND R. BRIAN, *Definition of a 5MW/61.5m wind turbine blade reference model*, SAND2013-2569 463454, 2013.
- [30] A. J. COULLING, A. J. GOUPEE, A. N. ROBERTSON, J. M. JONKMAN AND H. J. DAGHER, *Validation of a FAST semi-submersible floating wind turbine numerical model with DeepCwind test data*, *J. Renewable Sustainable Energy*, 5 (2013), 023116.
- [31] A. GASMI, M. A. SPRAGUE, J. M. JONKMAN AND W. B. JONES, *Numerical stability and accuracy of temporally coupled multi-physics modules in wind turbine CAE tools*, *AIAA Aerospace Sciences Meeting Including the New Horizons Forum & Aerospace Exposition*, 2013.
- [32] A. NING, R. DAMIANI AND P. MORIARTY, *Objectives and constraints for wind turbine optimization*, *J. Solar Energy Eng.*, 136 (2013), pp. 303–312.
- [33] B. R. RESOR AND D. C. MANIACI, *Definition of the national rotor testbed: an aeroelastically relevant research-scale wind turbine rotor*, *AIAA SciTech: 32nd ASME Wind Energy Symposium*, 2013.
- [34] E. BENINI AND A. TOFFOLO, *Optimal design of horizontal-axis wind turbines using blade-element theory and evolutionary computation*, *J. Solar Energy Eng.*, 124 (2002), pp. 357–363.
- [35] M. M. HAND, D. A. SIMMS, L. J. FINGERSH, D. W. JAGER, J. R. COTRELL, S. SCHRECK AND S. M. LARWOOD, *Unsteady aerodynamics experiment phase VI: wind tunnel test configurations and available data campaigns*, *National Renewable Energy Laboratory, Golden, CO, Report No. NREL/TP-500-29955*, 2001.
- [36] J. JONKMAN, S. BUTTERFIELD, W. MUSIAL AND G. SCOTT, *Definition of a 5MW reference wind turbine for offshore system development*, *National Renewable Energy Laboratory Tech Rep, NREL/TP-500-38060*, 2009.

- [37] X. QIU, J. X. XU, K. C. TAN AND H. A. ABBASS, *Adaptive cross-generation differential evolution operators for multiobjective optimization*, IEEE Trans. Evolutionary Comput., 20 (2016), pp. 232–244.
- [38] J. BADER AND E. ZITZLER, *HypE: An algorithm for fast hypervolume-based many-objective optimization*, Evolutionary Comput., 19 (2011), pp. 45–76.
- [39] F. T. BROOKS, D. S. POPE AND M. A. MARCOLINI, *Airfoil self-noise and prediction*, NASA Reference Publication, National Aeronautics and Space Administration, Office of Management, Scientific and Technical Information Division, NASA-RP-1218, 1989.
- [40] M. V. LOWSON, *Assessment and prediction model for wind turbine noise: basic aerodynamic and acoustic models*, Department of Trade and Industry, W/13/00284/REP, 1993.
- [41] P. MORIARTY AND P. MIGLIORE, *Semi-empirical aeroacoustic noise prediction code for wind turbines*, National Renewable Energy Laboratory Tech Rep, NREL-TP-500-34478, 2003.
- [42] H. KIM, S. LEE, E. SON, S. LEE AND S. LEE, *Aerodynamic noise analysis of large horizontal axis wind turbines considering fluid-structure interaction*, Renewable Energy, 42 (2012), pp. 46–53.
- [43] O. ANICIC, D. PETKOVIĆ AND S. CVETKOVIC, *Evaluation of wind turbine noise by soft computing methodologies: A comparative study*, Renewable Sustainable Energy Reviews, 56 (2016), pp. 1122–1128.
- [44] M. TÜRK AND S. EMEIS, *The dependence of offshore turbulence intensity on wind speed*, J. Wind Eng. Industrial Aerodyn., 98 (2010), pp. 466–471.